Journal Name

COMMUNICATION

Real-time imaging and local elemental analysis of nanostructures in liquids

Edward A. Lewis,[a] Sarah J. Haigh,*[a] Thomas J. A. Slater,[a] Zheyang He,[a] Matthew A. Kulzick,[b] Mary G. Burke [a] and Nestor J. Zaluzec [a,*c]

A new design of *in situ* liquid cells is demonstrated, providing the first nanometer resolution elemental mapping of nanostructures in solution. The technique has been applied to investigate dynamic liquid-phase synthesis of core-shell nanostructures and to simultaneously image the compositional distribution for multiple elements within the resulting materials.

Wet chemical processing routes provide a cost-effective method of synthesising a wide variety of nanocrystal structures, although controlling and predicting the shape and size-distributions of the resulting nanomaterials remains a challenge. A deeper understanding of liquid-phase nanocrystal growth mechanisms is highly desirable, but progress has been limited due to the difficulty of probing dynamic processes occurring within liquids. Recent advances in nanofabrication have produced liquid environmental-cell (e-cell) specimen holders for the transmission electron microscope (TEM),[1,2] allowing atomic resolution imaging of nanomaterials in liquid.[3,4] Real-time observations of nanocrystals in liquids have provided new insights into complex phenomena like nanoparticle growth and coalescence[3,5], but complementary elemental mapping of liquid phase systems was previously impossible.[6,7]

Liquid e-cell specimen holders for the TEM are fabricated with ultra-thin SiNx windows which sandwich specimens within a liquid or gaseous environment and are sufficiently thin to facilitate microstructural studies using the scanning/transmission electron microscope (S/TEM).[1,5] These windows serve to both protect the instrument vacuum and to prevent evaporation of the environmental media. While studies of dynamic nanoscale phenomena in a fluidic environment present new and exciting opportunities for materials research, a limitation of e-cell designs

has been that analytical spectroscopic techniques, which today have become standard tools for the characterization of nanomaterials in the S/TEM,8,9,10 are limited or virtually non-existent in e-cell studies.6 Two different factors dominate this shortcoming for electron energy loss and X-ray energy dispersive spectroscopy (EELS/XEDS) respectively. EELS has proved effective for measuring the nominal thickness of liquid layers and changes in the valence EELS spectra have been used to give insights into dynamic processes, for example the lithiation and delithiation of a battery cathode, occurring in e-cells.[6] However, high sensitivity electron energy loss spectroscopy can only be achieved when sufficiently small volumes of material are analysed; in a typical liquid e-cell the combined thickness of the SiNx windows, the probed sample, and surrounding environmental media is substantial and multiple inelastic scattering events dominate the electron energy loss signal, making elemental identification from core-loss EELS peaks challenging and spatially resolved elemental spectrum imaging impossible.6 X-ray energy dispersive spectroscopy suffers from a different limitation in e-cell studies which is purely geometrical in nature. The physical design of the e-cell holder prevents characteristic X-rays, emitted from the region of interest, from reaching the XEDS detector(s).[6,11] Due to this shortcoming, X-ray spectroscopy and elemental mapping has to-date been dismissed in e-cell experiments. This deficiency has recently been resolved by conscientious re-design of the e-cell holder,specifically the top plate of the e-cell holder was machined to remove material from key regions, reducing the extent to which X-rays were prevented from reaching the four detectors.11 In this work we demonstrate the first successful application of a modified e-cell holder to high-resolution elemental mapping in liquid at the 10 nm level. We show that when combined with a high brightness probe-corrected STEM and the latest generation of windowless, large collection angle X-ray detectors this technology provides a
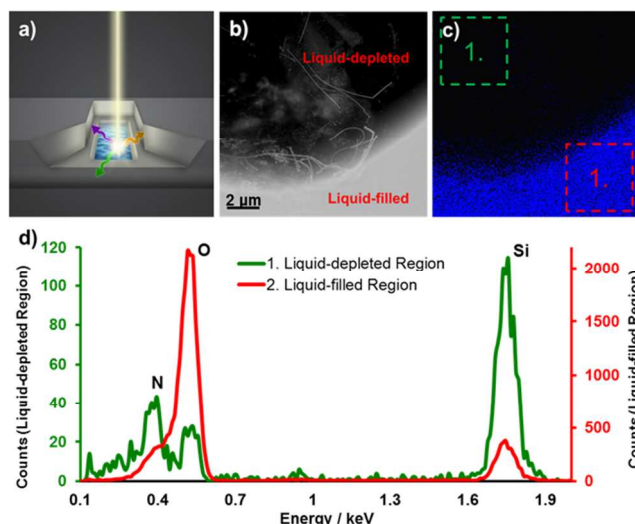
Fig. 1. (a) Schematic of the modified liquid e-cell TEM specimen holder (a detailed description of the holder design can be found in Ref. 11). (b) Contrast variation in HAADF STEM image due to the presence of liquid, the bright area in the lower right hand corner corresponds to a liquid-filled region, the darker area is a liquid-depleted region. (c) Shows the O K_α spectrum image. X-ray energy dispersive spectra from two regions of this spectrum image are shown in (d), note the large variation in O_K/Si_K peak ratios (4.78 vs 0.19 for liquid-filled and liquid-depleted areas respectively).

powerful tool for probing nanoscale chemical processes in fluids. We demonstrate that it is possible to simultaneously map the distribution of multiple elements at the nanoscale and to study the evolution of nanostructures as dynamic growth processes occur within the liquid.

As an exemplar, we have chosen to study an aqueous solution containing copper ions and a mixture of engineered nanostructures: silver nanowires (Ag-NWs), gold nanoparticles (Au-NPs), and palladium-decorated carbon nanotubes (Pd-CNTs). This nanoparticle "soup" was devised to provide a dynamic and chemically rich environment in which to test the limits of hyperspectral analysis of nanoparticles in liquid.

It is possible to identify regions of liquid by the greater electron scattering observed in the high angle annular dark field (HAADF) STEM image (Fig. 1b), by the visible motion of small nanoparticles (Video S7), by EELS t/λ measurements (Fig. S4), and by using a spectral signature measured using XEDS (Fig 1d). The latter method provides unambiguous evidence of water. Two spectra taken from different regions of the same hyperspectral image, one region is liquid-filled and the other is liquid-depleted, show a marked difference. The signature of water is identified by noting the K shell X-ray intensity ratio of oxygen (from water) to silicon (from the SiN_x windows); this ratio serves as an indication of the amount of water trapped between the SiN_x windows. Experimentally, we find that the O_K/Si_K intensity ratio on a reference (liquid-free) SiN_x window is nominally 0.024 ± 0.005 (Fig. S1). In contrast, the O_K/Si_K ratios measured in e-cells containing encapsulated liquid can be more than 100 times greater (Fig. S2). A large variation in O_K/Si_K ratios arises from variation in the amount of liquid present in different regions of the e-cell, due to both bowing of the windows and entrapped pockets of air.[6,12] Figure 1 shows that the
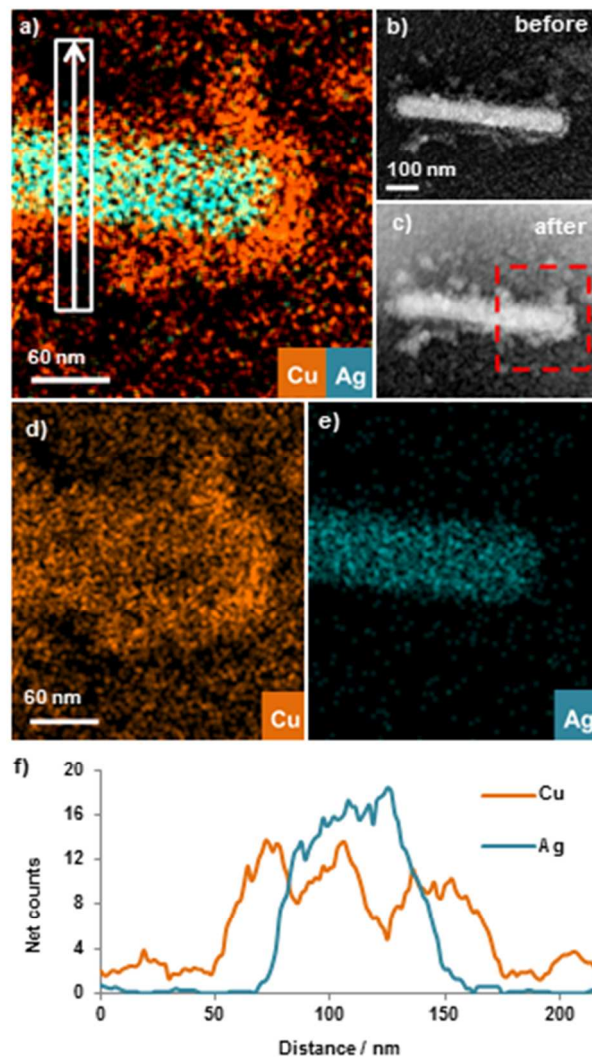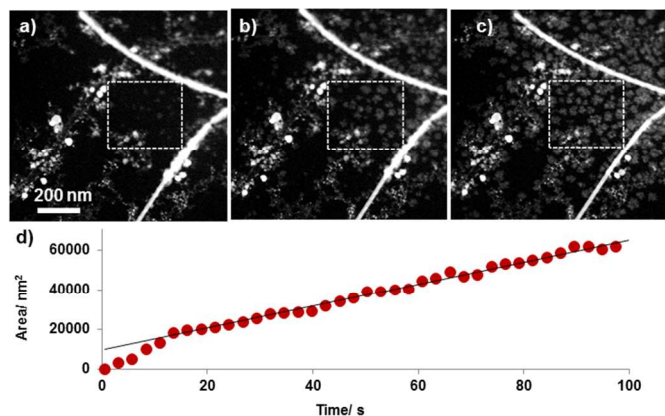

experimental O_K/Si_K ratios correlate directly with the variations in contrast

Fig. 2. A bimetallic nanostructure in water was imaged before (b) and after (c) XEDS data acquisition, nanoparticle deposition has clearly occurred on and around the Ag-NW during data acquisition. Elemental maps (a)(d) and (e) extracted from fhe XEDS spectrum image, for the region of interest indicated by the dotted line in (b), shows an Ag-NW coated in Cu nanoparticles. An X-ray line profile (f) extracted from the spectrum image shows elevated Cu concentration on and around the Ag-NW.

observed in the corresponding HAADF STEM images; when variable thickness liquid films are present within the same field of view, dramatic differences are correspondingly observed in the oxygen signal from disparate regions.

In Figure 2 we demonstrate liquid-phase spectral imaging by observing dynamic nanoscale Cu precipitation. *In situ* XEDS elemental mapping conclusively identifies the precipitation of Cu-rich species upon a silver nanowire (Fig. 2a,d) which was entirely immersed in liquid. Spectra from the region of interest show the presence of a large oxygen signal (O_K/Si_K ~2.8), verifying the presence of water. Using hyperspectral imaging and post-processing, we obtain a line profile (Fig. 2f) across the Cu-coated Ag nanowire in liquid, which succinctly demonstrates that a spatial resolution better than 15 nm is achievable.

Fig. 3. (a-c) show a sequence of HAADF STEM images taken at times t=0 s, t= 31.4 s, and t=62.9 s. This image sequence demonstrates beam-induced Cu nanoparticle growth in an area where pre-synthesised nanostructures (Ag-NWs and Pd-CNTs) are present (full image sequence available as Video S6). (d) shows the areal growth rate, calculated by image thresholding (Fig. S3).

The strong interaction of the electron beam with the media allows us to quantitatively study beam induced deposition of Cu metal from Cu ions in solution. There are a number of previous *in situ* liquid e-cell S/TEM studies in which solvated metal ions have been reduced by the electron beam to form metal nanostructures.[2,5,13,14] However, until now it has not been possible to unambiguously identify or measure the composition of the resulting structures without first removing them from solution. This current work mitigates this problem. Figure 3 illustrates the beam-induced growth of Cu nanoparticles in the presence of other pre-synthesised nanostructures (Video S6). Based on a sequence of scanned HAADF images, an estimated areal growth rate of 550 nm^2s^{-1} is calculated (Fig. S3). Cu deposition does not occur uniformly across the field of view, suggesting that the pre-existing nanostructures influence Cu growth.[14]

The spectral data in Figure 2 demonstrates that the Ag-NW is covered with an approximately 20 nm thick Cu coating formed during imaging in liquid containing Cu ions. Although the process of Cu deposition had commenced prior to starting the XEDS data acquisition, further Cu growth occurs during the acquisition of the spectrum images as is apparent from the differences in the appearance of the Ag nanowire in the pre- and post-acquisition HAADF images (Fig. 2b,c). The XEDS data therefore represents an average structure for the period of acquisition. Despite this, the elemental spectrum image provides vital information about the chemistry of this complex multicomponent system. No deposition is observed for imaging of a similar dry Ag-NW (Fig. S1), confirming that this reaction is a direct result of immersion in liquid containing Cu ions.

Figure 4 is a final example which establishes the power of elemental X-ray spectrum imaging during liquid e-cell experiments. This liquid immersed region contains a complete compendium of structures from our nanoparticle "soup" solution: Ag-NW, Au-NP, and Pd-CNT as well as copper deposited by the action of the electron beam. This area is less wet than that presented in Figure 2 with a lower O_K/Si_K count ratio of 0.85 compared to 2.77, this is, however, still more than 35x higher
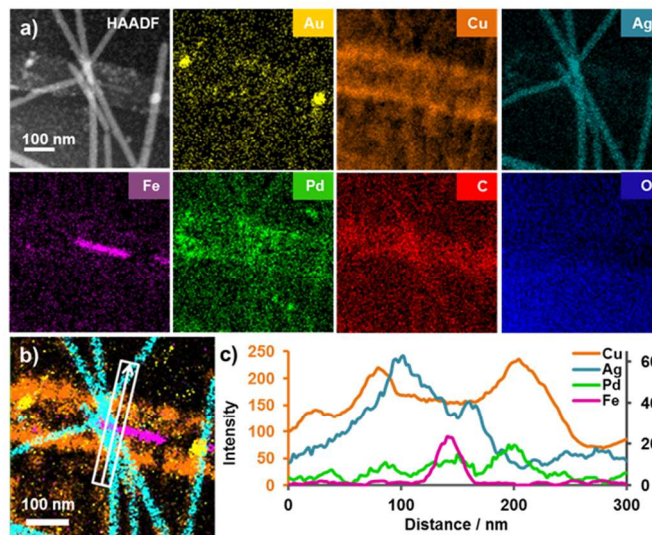
than the dry reference spectra. Only through the use of the elemental spectrum images is it possible to unambiguously interpret the HAADF image to distinguish the compositional distribution of the individual nanostructures present. From the XEDS data, it is clear that there are two ~40 nm diameter Au-NPs on either side of the image and that the Pd-CNT contains a distinct residual Fe catalyst core. The

Fig. 4. (a) HAADF STEM image and XEDS hyperspectral images demonstrating simultaneous mapping of multiple elements at the nanoscale in liquid. The full range of nanostructures can be clearly differentiated in the XEDS spectrum images (a). The HAADF image shown in (a) was taken before imaging, when little Cu deposition had occurred. The Cu deposition, which occurs during XEDS acquisition, is inhomogeneous with elevated Cu concentration along the outer walls of the Pd-CNT. The Cu coated outer walls and Fe core of the Pd-CNT can be seen in the line scan (c) taken from the region indicated in (b).

smallest nanoparticles (<10 nm) which surround the Ag-NWs and Pd-CNT are mainly copper deposited from solution. An elevated Cu signal is seen along the edges of the Pd-CNT; copper deposition appears to occur preferentially on surfaces, so this elevated Cu signal is simply a consequence of having a large surface area parallel to the electron beam direction in these regions (Fig. 4c).

Conclusions

This paper demonstrates a new technique capable of probing the local elemental compositions of nanocrystals in liquid. This provides the first means to directly observe and image nanoscale compositional changes occurring during wet chemical processes. Given that a great deal of nanomaterial synthesis and processing is achieved using wet chemistry and the improvements in nanomaterial properties possible with heterostuctured and alloyed nanomaterials,[9,15] we expect this new and powerful tool to yield many important insights in the field of nanoscience. We suggest that this technique will be invaluable in a range of applications: in catalysis, where it could lead to a better understanding of both the synthesis of catalytic nanomaterials and their performance and degradation while catalysing liquid-phase reactions;[10,16] in metallurgy, where corrosion processes

could be directly observed;[17] and in biology, where XEDS spectrum imaging could be applied to hydrated cells.[7,18]

Notes and references

a Materials Performance Centre and Electron Microscopy Centre, School of Materials, University of Manchester, Manchester, UK.
Email: sarah.haigh@manchester.ac.uk

b BP Corporate Research Center, Naperville, Illinois, USA.

c Electron Microscopy Center, Argonne National Laboratory, Argonne, USA.
Email: zaluzec@aaem.amc.anl.gov

† Electronic Supplementary Information (ESI) available. Contains experimental details of the electron microscopy performed in this work and figures demonstrating: HAADF STEM imaging and XEDS spectrum imaging of dry reference samples and wet samples; image thresholding to determine the areal growth rate of Cu nanostructures; EELS t/λ measurements to determine liquid thickness; and measurements of the tilt and position dependence of X-ray counts. Videos of beam-induced Cu deposition and the movement of a liquid wavefront are also available. See DOI: 10.1039/c000000x/

1   M. J. Williamson, R. M. Tromp, P. M. Vereecken, R. Hull and F. M. Ross, *Nat Mater*, 2003, **2**, 532.

2   H.-G. Liao, K. Niu and H. Zheng, *Chem Commun*, 2013, **49**, 11720.

3   J. M. Yuk, J. Park, P. Ercius, K. Kim, D. J. Hellebusch, M. F. Crommie, J. Y. Lee, A. Zettl and A. P. Alivisatos, *Science*, 2012, **336**, 61.

4   M. J. Dukes, B. W. Jacobs, D. G. Morgan, H. Hegde and D. F. Kelly, *Chem Commun*, 2013, **49**, 3007; Y. Liu, K. P. Tai and S. J. Dillon, *Chemistry of Materials*, 2013, **25**, 2927.

5   H. Zheng, R. K. Smith, Y.-w. Jun, C. Kisielowski, U. Dahmen and A. P. Alivisatos, *Science*, 2009, **324**, 1309; H. G. Liao, L. K. Cui, S. Whitelam and H. M. Zheng, *Science*, 2012, **336**, 1011; T. J. Woehl, C. Park, J. E. Evans, I. Arslan, W. D. Ristenpart and N. D. Browning, *Nano Letters*, 2013, **14**, 373.

6   M. E. Holtz, Y. Yu, J. Gao, H. D. Abruna and D. A. Muller, *Microscopy and Microanalysis*, 2013, **19**, 1027; K. L. Jungjohann, J. E. Evans, J. A. Aguiar, I. Arslan and N. D. Browning, *Microscopy and Microanalysis*, 2012, **18**, 621. M. E. Holtz, Y. Yu, D. Gunceler, J. Gao, R. Sundararaman, K. A. Schwarz, T. A. Arias, H. D. Abruña and D. A. Muller, *Nano Letters*, 2014, **14**, 1453.

7   C. Wang, Q. Qiao, T. Shokuhfar and R. F. Klie, *Advanced Materials*, 2014.

8   S. J. Haigh, A. Gholinia, R. Jalil, S. Romani, L. Britnell, D. C. Elias, K. S. Novoselov, L. A. Ponomarenko, A. K. Geim and R. Gorbachev, Nat Mater, 2012, **11**, 764; K. A. Dick, J. Bolinsson, B. M. Borg and J. Johansson, Nano Letters, 2012, **12**, 3200;   C. Shankar, A. T. Dao, P. Singh, K. Higashimine, D. M. Mott, S. Maenosono, Nanotechnology, 2012, **23**, 245704; M. A. Van Huis, A. Figuerola, C. Fang, A. Béché, H. W. Zandbergen and L. Manna, Nano Letters, 2011, **11**, 4555; J. H. Lee, J. T. Jang, J. S. Choi, S. H. Moon, S. H. Noh, J. W. Kim, J. G. Kim, I. S. Kim, K. I. Park and J. Cheon, Nature Nanotechnology, 2011, **6**, 418.

9   H. L. Xin, J. A. Mundy, Z. Liu, R. Cabezas, R. Hovden, L. F. Kourkoutis, J. Zhang, N. P. Subramanian, R. Makharia, F. T. Wagner and D. A. Muller, *Nano Letters*, 2012, **12**, 490.

10 D. Wang, H. L. Xin, R. Hovden, H. Wang, Y. Yu, D. A. Muller, F. J. DiSalvo and H. D. Abruna, *Nature Materials*, 2013, **12**, 81.

11 N. J. Zaluzec, M. G. Burke, S. J. Haigh and M. A. Kulzick, *Microscopy & Microanalysis*, 2014, **20**, 323.

12 J. M. Grogan, N. M. Schneider, F. M. Ross and H. H. Bau, Nano Letters, 2013, **14**, 359.

13 L. R. Parent, D. B. Robinson, T. J. Woehl, W. D. Ristenpart, J. E. Evans, N. D. Browning and I. Arslan, *ACS Nano*, 2012, **6**, 3589; T. J. Woehl, J. E. Evans, L. Arslan, W. D. Ristenpart and N. D. Browning, *Acs Nano*, 2012, **6**, 8599.

14 K. L. Jungjohann, S. Bliznakov, P. W. Sutter, E. A. Stach and E. A. Sutter, *Nano Letters*, 2013, **13**, 2964.

15 W. Ma, J. M. Luther, H. Zheng, Y. Wu and A. P. Alivisatos, *Nano Letters*, 2009, **9**, 1699; L. Britnell, R. V. Gorbachev, R. Jalil, B. D. Belle, F. Schedin, A. Mishchenko, T. Georgiou, M. I. Katsnelson, L. Eaves, S. V. Morozov, N. M. R. Peres, J. Leist, A. K. Geim, K. S. Novoselov and L. A. Ponomarenko, *Science*, 2012, **335**, 947.

16 Xin, E. A. Pach, R. E. Diaz, E. A. Stach, M. Salmeron and H. Zheng, *ACS Nano*, 2012, **6**, 4241; S. Zhang, L. Nguyen, Y. Zhu, S. Zhan, C.-K. Tsung and F. Tao, *Accounts of Chemical Research*, 2013, **46**, 1731.

17 S. R. K. Malladi, F. D. Tichelaar, Q. Xu, M. Y. Wu, H. Terryn, J. M. C. Mol, F. Hannour and H. W. Zandbergen, *Corrosion Science*, 2013, **69**, 221.

18 D. B. Peckys, G. M. Veith, D. C. Joy and N. de Jonge, *Plos One*, 2009, **4**; M. J. Dukes, D. B. Peckys and N. de Jonge, *Acs Nano*, 2010, **4**, 4110; B. L. Gilmore, S. P. Showalter, M. J. Dukes, J. R. Tanner, A. C. Demmert, S. M. McDonald and D. F. Kelly, *Lab on a Chip*, 2013, **13**, 216.